Journal of Materials Chemistry A

Nanoporous Gyroid Ni/NiO/C Nanocomposite from Block Copolymer Template with High Capacity and Stability for Lithium Storage

Journal:	*Journal of Materials Chemistry A*
Manuscript ID	TA-ART-05-2018-004077.R1
Article Type:	Paper
Date Submitted by the Author:	11-Jun-2018

Complete List of Authors:	Cheng, Chung-Fu; The University of Akron, Department of Polymer Science Chen, Yu-Ming; University of Akron, Department of Polymer Science Zou, Feng; University of Akron, Department of Polymer Science Yang, Kai-Chieh; National Tsing Hua University, Chemical Engineering Lin, Tzu-Ying; National Tsing Hua University, Materials Science and Engineering Liu, Kewei; The University of Akron, Department of Polymer Science Lai, Chih-Huang; National Tsing Hua University, Department of materials science and engineering Ho, Rong-Ming; National Tsing-Hua University, Department of Chemical Engineering Zhu, Yu; The University of Akron, Department of Polymer Science

Nanoporous Gyroid Ni/NiO/C Nanocomposite from Block Copolymer Template with High Capacity and Stability for Lithium Storage

Chung-Fu Cheng[1], Yu-Ming Chen[1], Feng Zou[1], Kai-Chieh Yang[2], Tzu-Ying Lin[3], Kewei Liu[1], Chi-Huang Lai[3], Rong-Ming Ho[2]* and Yu Zhu[1]*

[1]*Department of Polymer Science, University of Akron, Akron, Ohio 44325 USA*
[2]*Department of Chemical Engineering, National Tsing Hua University, Hsinchu 30010, Taiwan*
[3] *Department of Materials Science and Engineering, National Tsing Hua University, Hsinchu 30010, Taiwan*

**Email - yu.zhu@uakron.edu*

Nanoporous Ni/NiO/C nanocomposite with gyroid nanostructure was fabricated by using a nanoporous polymer with gyroid nanochannels as a template. The polymer template was obtained from the self-assembly of degradable block copolymer, polystyrene-*b*-poly(L-lactide) (PS-PLLA), followed by the hydrolysis of PLLA blocks. Templated electroless plating followed by calcination was conducted to create precisely controlled Ni/NiO gyroid nanostructure. After carbon coating, well-interconnected nanoporous gyroid Ni/NiO/C nanocomposite can be successfully fabricated. Benefiting from the well-interconnected nanoporous structure with ultrafine transition metal oxide and uniform carbon coating, the gyroid nanoporous Ni/NiO/C nanocomposite electrodes exhibited high specific capacity at various rates (1240 mAh/g at 0.2 A/g, 902 mAh/g at 2 A/g and 424 mAh/g at 10 A/g) and excellent cyclability (809 mAh/g at 1 A/g after 1000 cycles, average Coulombic efficiency 99.86%). This research demonstrated a universal approach for constructing nanostructured electrode with explicitly controlled block copolymer phase separation.

Keywords: Lithium Ion Battery, Block Copolymers, Nanocomposite, Nanoporous Materials, Electroless Plating, Templates, Gyroid

Introduction

With the increased energy demand from the emerging technologies such as wearable electronics and electricity powered vehicles, various functional high-efficiency energy storage devices have attracted extensive attention in recent years.[1-6] Among the electrochemical energy storage devices, lithium ion batteries (LIBs) are highly desirable in portable electronic devices as well as greener automobiles including electric vehicles (EVs) and hybrid electric vehicles (HEVs).[7-12] Nevertheless, the commercial graphite anode exhibits a relatively low theoretical specific capacity of 372 mAh/g, which is no longer able to fulfill the requirements of emerging applications as EVs, where higher energy density and power density are of paramount importance. In order to increase the energy density and power density of LIBs, novel anode nanomaterials with lower cost, higher specific capacity, and better durability as well as ratability are urgently needed. Transition metal oxides (MO_x, M = Mn, Fe, Ni, Co, Sn, etc.), as emerging conversion-reaction type anode materials, are appealing candidates due to their higher specific capacities (~1000 mAh/g) compared to intercalation anode like graphite.[13-19] Furthermore, within the transition metal oxide category, nickel oxide-based nanomaterials are one of the most studied systems due to its high lithium storage capacity.[20-25] However, the performance of nanostructured NiO anode has been limited by its poor electrical conductivity and large volume variation upon lithiation and de-lithiation.[26,27] Various methods have been carried out to accommodate the volume expansion phenomenon and enhance the electrical conductivity. For instance, successful nanostructure engineering of transition metal oxide materials has been demonstrated in lithium ion batteries[14, 28-30] to mitigate the volume-change-induced mechanical strain. Additionally, hybridization with

carbonaceous materials (graphene, graphene oxides, carbon nanotubes, or conductive polymers) has been used to enhance the conductivity of the transition metal oxide electrode.[31-34] Another straightforward route to fabricate nanostructured NiO with carbonaceous hybrid materials is to directly deposit desired NiO-based materials into templates with defined nanochannels through templated syntheses using nanostructured carbon or nanoporous polymer as a template.[35-38]

In recent decades, block copolymers (BCPs) have been comprehensively investigated because of their capability to self-assemble into one-, two-, and three-dimensional periodic nanostructures while being readily adjustable in size, which is dependent upon their constituted compositions and molecular weights.[39,40] Moreover, the degradable characters of BCPs is advantageous because it enables the synthesis of nanoporous polymers with well-ordered texture by simply removal of degradable component(s) in BCPs through hydrolysis[41-43], ozonolysis,[44] UV degradation,[45] reactive ion etching[46] or hydrofluoric acid etching[47]. In addition, the nanoporous polymers with well-defined nanochannels, in particular, for gyroid-structured phase from the self-assembly of BCPs, can be used as templates for templated synthesis.[48] By exploiting the templating process, reactions such as atomic layer deposition,[49,50] electrochemical deposition,[51-53] electroless plating,[54-57] and sol-gel reaction[58-60] can be carried out using the BCP templates for the fabrication of nanoporous inorganic materials with precisely controlled morphology after removal of the polymer template.

Herein, a new approach was proposed for the fabrication of nanoporous gyroid Ni/NiO/C nanocomposite with a well-defined morphology (*i.e.*, gyroid-forming nanostructure). The well-ordered network structures are of particular interest as they exhibit excellent

performance in mitigating the volume expansion.[61] The continuous gyroid structure also provides ideal electron transport channel (through the structure of gyroid itself) and ion transport channel (through the continuous voids of gyroid matrix) for the electrode, enhancing the power of the electrode. The nanoporous gyroid nanocomposite was synthesized starting from using hydrolyzed polystyrene-*b*-poly(L-lactide) (PS-PLLA) to prepare nanoporous PS template with gyroid-forming nanochannels,[54-60] followed by templated electroless plating of Ni to form PS/Ni nanohybrids. In order to convert the Ni-based gyroid structure into conductive electrode material, a modified two-step calcination process was incorporated in this study. The main purpose is to thermally decompose the PS template with well-preservation of the gyroid structure and to post oxidize the Ni into NiO. It must be noted that severe collapse may occur if the PS template is drastically removed. Therefore, it is necessary to attune the ramping temperature process for removal of the PS template and oxidation of Ni, in order to prevent the drastic deformation of the nanostructure. After removal of the PS template and the further oxidation of Ni, a subsequent carbon coating procedure was performed to enhance the conductivity. This nanoporous gyroid-structured Ni/NiO/C nanocomposite is an ideal anode material for the high-performance lithium-ion battery as it possesses well-interconnected nanoporous structure with ultrafine transition metal oxide nanonetwork and uniform carbon coating. These desirable features enable the subsequently fabricated electrodes to exhibit high specific capacity while simultaneously provide excellent electrical conductivity and robust structure. Consequently, the LIB with this novel anode exhibits an extremely long cycle life of 1000 cycles at a current density of 1 A/g and excellent rate performance. To the best of our knowledge, Ni/NiO/C nanocomposite with

a well-ordered unique nanoporous gyroid structure serving as an anode in LIB, giving such outstanding performance and cyclability, has not been previously reported.

Experimental Section

Synthesis of PS-PLLA

Detailed synthetic strategy and routes of the PS-PLLA sample were described in previously published results.[54,55] Generally, the PS-PLLA was synthesized by atomic transfer radical polymerization (ATRP) using doubled headed initiator. GPC was further utilized to characterize the number-average molecular weight and polydispersity index (PDI) of the product. The PDI of synthesized PS-PLLA was then further determined and the repeated unit number of L-LA versus PS were determined by ^{1}H NMR analysis. In this study, the number-average molecular weights of the PS, the PLLA and the PDI of the PS-PLLA are 34000 g mol^{-1}, 27000 g mol^{-1} and 1.21, respectively. For the given densities of PS and PLLA (1.02 and 1.248 g/cm^3, respectively), the volume fraction of PLLA, f_{PLLA}^{v}, is then calculated as 0.37.

Preparation of Block Copolymer Template

Solution casting was carried out to prepare bulk samples of PS-PLLA with dichloromethane (CH_2Cl_2) as solvent (10 wt % of PS-PLLA) at room temperature. The samples were set for two weeks, and then dried in a vacuum oven at 65^{o}C for three days. With an aim to eliminate the residual PLLA crystals, the dried samples were heated to the maximum annealing temperature, T_{max}=175^{o}C for three minutes. After quenching (by using liquid nitrogen) the microphase-separated ordered melt at 175^{o}C, the samples were used for SAXS experiments. To prepare nanoporous PS template with gyroid

nanochannel, hydrolysis of PLLA blocks from the PS-PLLA samples was carried out by using a 0.5 M basic solution that was prepared by dissolving 2 g of sodium hydroxide in a 40/60 (by volume) solution of methanol/water. After three days of hydrolysis to complete the removal of PLLA, the hydrolyzed samples were rinsed with a mixture of DI water and methanol, and then used as templates for following experiments.

Templated Electroless Plating of Ni

The nanoporous PS templates with interconnected air networks were soaked in seeding aqueous solution mixed with methanol (12 mL) and $PdCl_2$ (0.01~0.02 g) with stirring at room temperature for 3~4 hours. After washing gently with methanol/H_2O solution to remove redundant Pd ions covering on sample surfaces, the pore-filled samples were immersed into a hydrazinium hydroxide (85%, 4 ml) methanol solution for the nucleation of Pd. With the control of low enough Pd ion concentrations, suitable amount of Pd nuclei within the nanochannels of the template can be formed. Subsequently, a fresh aqueous solution consisting of $NiCl_2$ (0.4 g), hydrazinium hydroxide (4 ml), ammonium hydroxide (6.4 ml), DI water (40 ml) and methanol (40 ml) was prepared and then the pre-treated templates with low content of Pd nuclei were immersed into the prepared solution. Accordingly, Ni ions were reduced to Ni clusters arising from pre-formed Pt nuclei so as to gradually develop within the nanochannels through the growth process and eventually formed the PS/Ni nanohybrids with preserved gyroid texture.

Formation of nanoporous gyroid Ni/NiO nanocomposite

To produce the nanostructured Ni/NiO nanocomposite, the PS template of the PS/Ni nanohybrids were degraded and oxidized by modified calcination under air purge. The

temperature was first increased to 350 ^{o}C and kept for 1 hr for further stabilization. After that, the temperature was then increased to 450^{o}C. Finally, the temperature was further kept at 550 ^{o}C for 5 hr to complete the PS removal. In the second oxidation stage, the temperature was then decreased to 450 ^{o}C and stabilized for 1 hr. After that, the temperature was decreased to 350 ^{o}C for 1 hr and then decreased to room temperature. Consequently, the nanostructured Ni/NiO materials were obtained.

Carbon coating

Carbon coating was performed by atmospheric pressure chemical vapor deposition (CVD). Acetylene was used as carbon source and the reaction temperature is 450 ^{o}C. A continuous argon purge was used during the carbon coating process. The sample was loaded in a ceramic boat and the coating time is 5 min. The flow rate of acetylene and argon is 4 and 200 sccm, respectively.

Battery Fabrication

The nanoporous gyroid Ni/NiO/C nanocomposite was mixed with carbon black and PAA at a weight ratio of 7:2:1, respectively. The addition of NMP and subsequent mixing by pestle and mortar produced a homogenous thick slurry. The mixture slurry was casted on a copper foil using a doctor blade. The casted electrode was placed in a vacuum oven at 50^{o}C overnight to remove solvent. 2032 coin cells were used for the fabrication of half cells. The fabrication of the cells was conducted in an Ar glovebox. Lithium metal was implemented as the counter electrode, Celgard 3501 as the separator. The electrolyte is 1 M lithium hexafluorophosphate solution in EC and DEC (1:1 v/v) with 10 wt %

fluoroethylene carbonate. The electrodes were punched into 5/16 circular discs, typically with a mass loading of 0.4–0.6 mg/cm^2

3. Results and Discussions

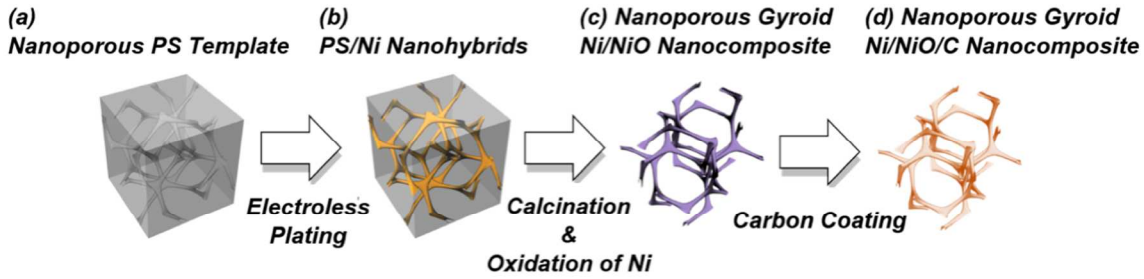

Figure 1. Schematic illustration of fabricating nanoporous gyroid Ni/NiO/C nanocomposite using polymer template from self-assembled degradable BCPs: (a) Nanoporous gyroid PS; (b) PS/Ni nanohybrids via templated electroless plating; (c) Removal of PS and oxidation of Ni with controlled calcination. (d) Nanoporous gyroid Ni/NiO/C nanocomposite after carbon coating.

The fabrication procedure of the Ni/NiO/C nanocomposite with nanoporous gyroid structure is illustrated in Fig. 1. A PS-PLLA with a molecular weight of 61,000 g/mol and a PLLA volume fraction of 37% was synthesized, following the previous reports.[37,38] A gyroid-forming phase consisting of co-continuous PLLA networks in a PS matrix can be formed after solution casting of the synthesized PS-PLLA followed by quenching from microphase-separated melt. One-dimensional small-angle X-ray scattering (1D SAXS) profile (curve (i) in Fig. 2(a)) confirms the formation of gyroid phase from the self-assembly of the PS-PLLA at which reflections are found at the relative q values of $\sqrt{6}$: $\sqrt{8}$:$\sqrt{14}$:$\sqrt{16}$:$\sqrt{32}$. The inter-domain spacing of the $(211)_{gyroid}$ ($d_{(211)G}$) was determined as approximately 51.2 nm from the primary reflection, suggesting a cubic unit cell of

119.7 nm for the forming gyroid phase. Fig. 2(a) displays the 1D SAXS profile of the PS-PLLA after hydrolysis (curve (ii)); the reflections at the relative q values remain unchanged as compared to curve (i) in Fig. 2(a), reflecting the preservation of the gyroid phase after hydrolytic treatment, suggesting that the PLLA networks can be selectively removed. As a result, the PS matrix with well-defined, bi-continuous nanochannels can be fabricated, and then employed as a template for following electroless plating of Ni. Corresponding One-dimensional wide-angle X-ray diffraction (1-D XRD) profile shown in Fig. S1 (c) confirmed the formation of Ni in the PS matrix.

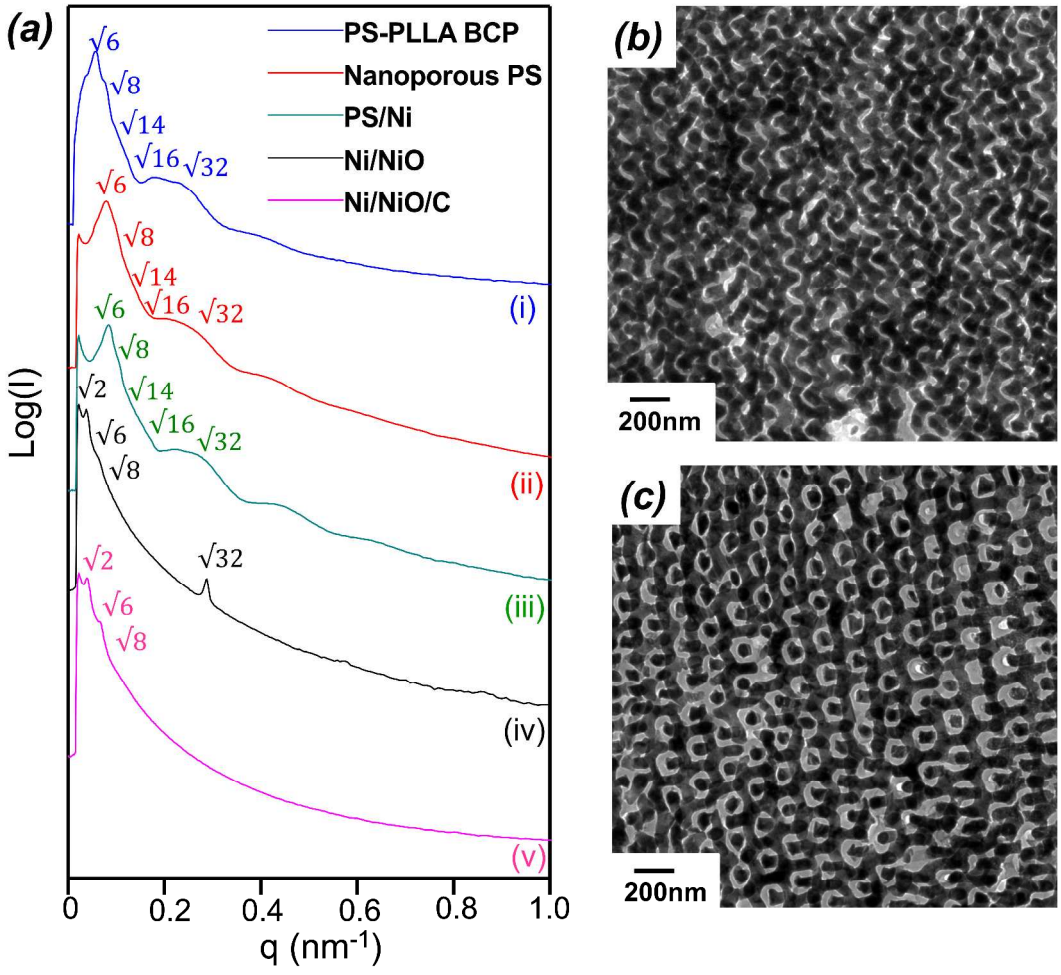

Figure 2. Nanostructural Characterization (a) 1D Small angle X-ray scattering (SAXS) profiles of (i) Self-assembled PS-PLLA BCPs; (ii) Nanoporous PS template after removal of the PLLA blocks in PS-PLLA BCP by hydrolysis; (iii) PS/Ni gyroid-structured nanohybrids; (iv) Nanoporous gyroid Ni/NiO nanocomposite; (v) Nanoporous gyroid Ni/NiO/C nanocomposite. (b) TEM micrographs of the PS/Ni nanohybrids with projection planes along [211] direction of gyroid structure. (c) TEM micrographs of the PS/Ni nanohybrids with projection planes along [100] direction of gyroid structure. The dark contrast represents for the Ni while the white contrast represents for the PS.

To acquire high conversion of Ni to NiO, a 2nd stage calcination was conducted by controlling the treated temperature (from 550^{o}C to room temperature), the diffusion of oxygen into nanoporous Ni will occur after removal of the PS template, giving rise to the acquired degree of thermal oxidation of Ni. As shown in Fig. 3(a), all the diffractions can be indexed as fcc (both Ni and NiO) based on JCPDS card no. 04-0850 and no. 47-1049, respectively. The lattice constant was calculated by first diffraction peak with a_{Ni} =3.520 Å and a_{NiO} = 4.171 Å. Note that all diffractions can be well indexed as the reflections of (111) and (200) for Ni, and (111), (200) and (220) for NiO, suggesting that nanoporous gyroid Ni/NiO nanocomposite can be trustfully fabricated after the designed thermal processes for calcination. As shown in Fig. 3(b), the FESEM micrograph depicts the unique gyroid texture with tripod and three-fold symmetry after the calcination, indicating that well-ordered nanonetworks for the nanoporous gyroid NiO/Ni nanocomposite was successfully fabricated. High-resolution TEM (HRTEM) was utilized to prove the crystalline lattice in real space. Fig. 3(d) displays the lattice fringes of Ni and NiO grain. The (111) and (200) reflections of Ni and the (200) reflection of NiO (Figs

3(e,f)) are in line with the calculated results from XRD (Fig. 3(a)). Also, Fig. 3(f) shows a clear interface between Ni and NiO, suggesting the formation of Ni/NiO nanocomposite. Furthermore, X-ray photoelectron spectroscopy (XPS) was used to examine the elemental composition of the nanoporous gyroid Ni/NiO nanocomposite (Fig. S4). The results also confirmed that a significant oxygen content was observed. As a result, the degeneration of the PS template and the thermal oxidation of Ni should be successfully achieved by the designed thermal processes for calcination to give the nanoporous gyroid Ni/NiO nanocomposite. The structure of the nanoporous gyroid Ni/NiO nanocomposite can be further identified by SAXS (curve (iv) in Fig. 2(a)); the reflections at the relative q values of $\sqrt{2}$:$\sqrt{6}$:$\sqrt{8}$:$\sqrt{32}$ can be found. Note that the appearance of the $\sqrt{2}$ peak is attributed to the formation of network shifting resulting from removal of the PS template, giving single gyroid like scattering with reflections similar to a space group of $I4_132$.[58,62] Although the characteristic reflections for the samples containing Ni/NiO at high q range are relatively broad, the identification of the gyroid nanostructure can be verified by corresponding SAXS results consisting of the reflections at a q ratio of $\sqrt{2}$ and $\sqrt{6}$.

Carbon coating has been proved as an effective method to improve the stability of nanomaterial electrode.[32,53,63] With conformal carbon coating, the electrode made from this conversion reaction materials will not only have high specific capacity but also possess stable SEI layer, excellent electrical conductivity, and robust structure. To fulfill the requirement of the high stability of the nanoporous gyroid Ni/NiO nanocomposite fabricated, carbon coating was performed to fabricate nanoporous gyroid Ni/NiO/C nanocomposite via chemical vapor deposition (CVD) using acetylene as carbon source (See supporting information for details). As shown in Fig. 3(c), the FESEM micrograph

displays the nanostructure of the nanoporous gyroid Ni/NiO/C nanocomposite after carbon coating. The structure of the nanoporous gyroid Ni/NiO/C can be further identified by SAXS (curve (v) in Fig. 2(a)); the reflections at a q ratio of $\sqrt{2}$ and $\sqrt{6}$ can be verified, suggesting that the well-ordered nanonetworks with gyroid structure can be well-preserved after the carbon coating. The forming nanonetworks can be in a long-range order as shown in Fig. S5 for the FESEM observation in low magnification. Also, the nitrogen adsorption/desortion isotherm at 77 K was performed to inestigate the specific surface area of the nanoporous gyroid Ni/NiO/C nanocomposite. As shown in Fig. S6 (a), the nanoporous gyroid Ni/NiO/C nanocomposite shows a a Brunauer – Emmett – Teller (BET) specific surface area of approximately 18.7 m^2/g. As confirmed by the pore size distribution (Fig. S6 (b)), the corresponding average pore size was about 18.8 nm.

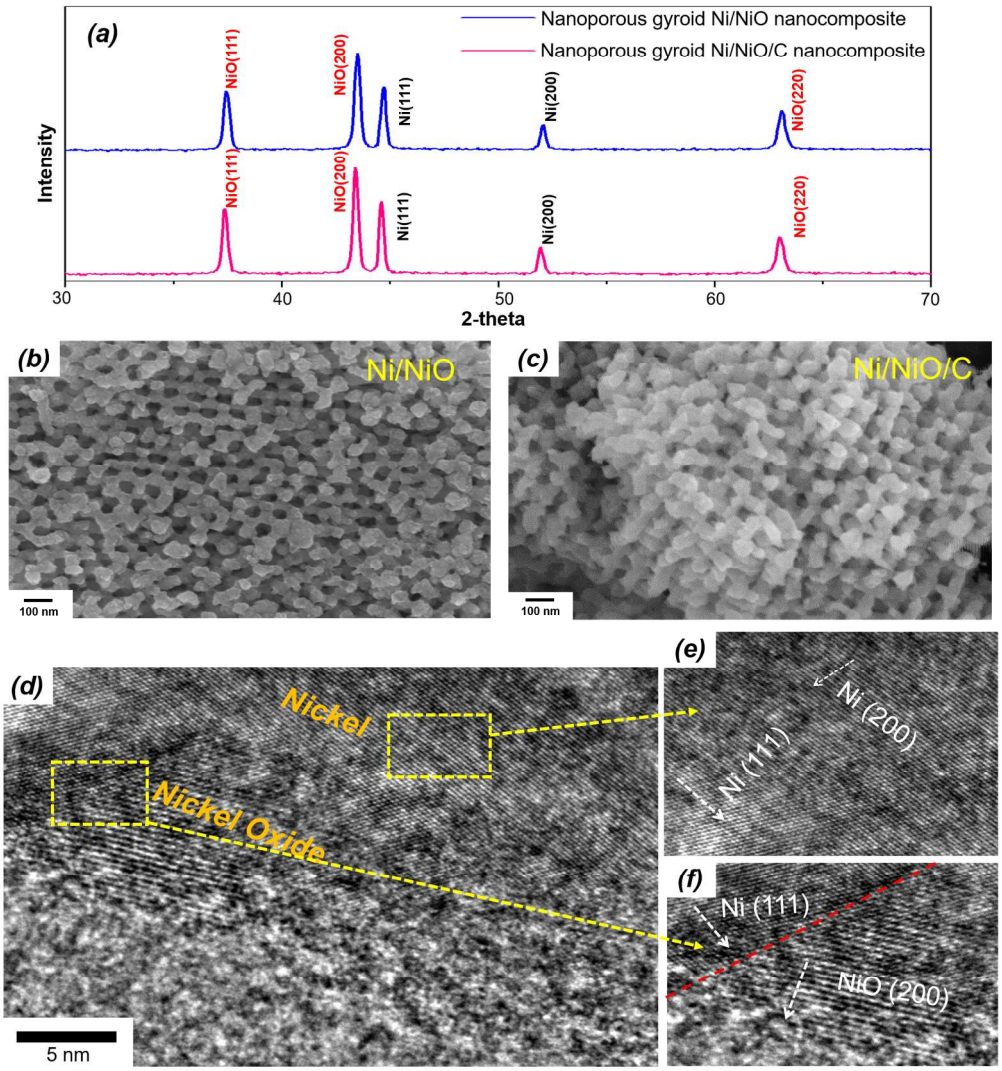

Figure 3. Characterization of nanoporous gyroid Ni/NiO and Ni/NiO/C nanocomposite (a) One-dimensional X-ray diffraction (XRD) profiles of the nanoporous gyroid NiO/Ni nanocomposite and Ni/NiO/C nanocomposite; the diffraction peaks of Ni are indexed as black while the peaks of NiO are index as red. (b, c) Field emission scanning electron microscope (FESEM) micrographs of the nanoporous gyroid Ni/NiO nanocomposite (b) and Ni/NiO/C nanocomposite after carbon coating (c). (d-f) HRTEM micrographs of the nanoporous gyroid Ni/NiO nanocomposite. (f) The enlarged area shows the lattice fringes

and the arrows show the directions for the grains of the Ni and (g) shows the interface of Ni and NiO.

Furthermore, as evidenced by the WAXD (Fig. 3(a)), the forming NiO can be well preserved after the formation of carbon coating at which the diffraction peaks of NiO remain unchanged. XPS was used to examine the elemental composition of the nanoporous gyroid Ni/NiO/C nanocomposite (Fig. S7). As validated by the Ni 2p XPS results (Fig. S8 (a)), which displays four peaks: $2p_{3/2}$ (854.9 eV and 862.1 eV) as well as $2p_{1/2}$ (873.3 eV and 880.1 eV). Compared with previous XPS results of NiO[64] and $Ni(OH)_2$[65], it was concluded that the surface of materials could be the $Ni(OH)_2$ coated NiO.[66] Since the formation of NiO is through the oxidation by oxygen in air, it is expected that NiO instead of Ni is dected by suface characterization method like XPS. However, XRD results indicated that majority of the materials is NiO and Ni. The $Ni(OH)_2$ detected from XPS could result from the hydrolyzation of smaples during the short exposure to air. The value of the binding energy difference between Ni $2p_{3/2}$ and Ni $2p_{1/2}$ is about 18.4 eV, which reveals the presence of NiO.[67, 68] The formation of C and O characteristic peaks after the carbon coating were displayed in Figs S8 (b) and (c), reflecting that the nanoporous Ni/NiO/C nanocomposite can be well prepared. The composition of C and NiO of the nanoporous gyroid Ni/NiO/C nanocomposite was determined by thermogravimetric analysis (TGA) (Fig. S9). On the basis of the TGA result, the compositions of Ni, NiO and C are about 13%, 74% and 13%, respectively. Such thin, conformal carbon coating is of pivotal importance for lithium ion battery (LIB) because it not only provides high conductivity for the transition metal network but also

improves the formation of a stable SEI layer, without sacrificing significant amount of capacity.[21]

Electrochemical properties of nanoporous gyroid Ni/NiO/C nanocomposite anode. To systematically investigate the electrochemical performance of the nanoporous gyroid Ni/NiO/C nanocomposite, LIB half cells using the nanoporous gyroid Ni/NiO/C nanocomposite and lithium metal counter electrode were fabricated. Cyclic voltammetry (CV) measurement was performed under a scan rate of 0.2 mV/s within the voltage range of 0.005−3 V vs. Li/Li^+. Fig. 4(a) depicts the first four cycles of the cyclic voltammetry (CV). In the first cathodic process, the peak at 0.2 V is attributed to the formation of SEI film and the reduction of NiO to metallic Ni, and the peak at 1.0 V can be referred as the generation of Li_2O. There are two broad oxidation peaks in the following anodic process; the one at 2.2 V is due to the reversible oxidation of Ni to NiO ($Ni + Li_2O \rightarrow NiO + 2Li^+ + 2e^-$), and the other at 1.7 V is caused by the partial decomposition of SEI components.[68] The overall electrochemical reaction of the nanoporous gyroid Ni/NiO/C nanocomposite electrode can be described in the following equation:

$$NiO + 2Li^+ + 2e^- \Leftrightarrow Ni + Li_2O \qquad \text{(eq 1)}$$

In the subsequent cycles, reduction peaks shift to about 1.1 V and oxidation peaks slightly shift to about 2.3 V and 1.6 V. These two redox reactions of lithium ions with the electrode are highly reversible. The difference between the equivalent peaks in the first cycle and subsequent cycles can be ascribed to the formation of SEI layer on the carbon surface.[69,70]

Fig. 4(b) shows the representative discharge-charge profiles of the nanoporous gyroid Ni/NiO/C nanocomposite electrode at various current densities. The electrode exhibits a

potential plateau at 0.7 V during the first discharge (0.2 A/g). After the first cycle, this long potential plateau is replaced by a long-sloped curve from 1.7 to 0.9 V, which is a typical phenomenon observed in conversion reaction electrode. In addition, the first discharge and charge profiles delivered specific capacities of 1754 and 1240 mAh/g, respectively. The capacity loss of 29.3% is mainly attributed to the interfacial reaction between NiO and the electrolyte.[18,22,24] As expected, the increase in current density gives rise to higher overpotential, resulting from the kinetic effects of the electrode materials, in terms of lower discharge plateau and higher charge potential. However, the discharge and charge curves under different rates still display a similar curve shape. The nanoporous gyroid Ni/NiO/C nanocomposite electrode also exhibits an impressive rate capability. Fig. 4(c) shows the rate capability behavior over 90 cycles from 0.2 A/g to 10 A/g. The discharge specific capacities are 1242, 1154, 1023, 902, 674 and 424 mAh/g at 0.2, 0.4, 1, 2, 4 and 10 A/g, respectively. Notably, even after cycling at a relatively high current density at 10 A/g (i.e., C rate = 14 C), the capacity can recover in proximity to its corresponding value when the current density is set back to 2 A/g and 0.4 A/g. Furthermore, when the current density is set back to the initial rate (0.2 A/g), the capacity can almost recover to the original value (i.e., the specific capacity is 1214 mAh/g for recover cycle). Notably, in contrast to the reported results of NiO-based electrode,[20-24] the nanoporous gyroid Ni/NiO/C nanocomposite exhibits better rate performance (Fig. S10). It is worth to note that the specific capacity achieved here is even higher than the theoretical capacity of NiO (718 mAh/g) based on the conversion reaction mechanism. We believe the additional capacity was achieved through the lithium storage on the nanoscale interface and partially reversible SEI decomposition.[71] The gyroid

nanostructure would be an ideal case for the lithium storage in the nanoscale interface, which is also observed in previous reports where the nanoporous transition metal oxide electrodes were used.[20, 23] The oxidation peak at 1.6 V from CV of the anode (Fig. 4(a)) is corresponding to partial decomposition of the anode.[21] To further understand the enhancement in specific capacity from the gyroid nanostructure, Ni/NiO/C composite materials with sheet-film morphology (see SI for detailed preparation) were also prepared and characterized (Fig S11(a,b)). The sheet-film Ni/NiO/C composite materials were tested in the batteries as well and the results are shown in Fig 4c and Fig. S11(c,d). As shown in Fig. 4(c), the rate performance indicated that the random structured Ni/NiO/C sheet-film composite anode exhibited significantly lower specific capacity as compared to the nanoporous gyroid Ni/NiO/C nanocomposite anode under all current densities, particularly at high C-rate cycles. We speculate that the excellent rate capability performance of the nanoporous gyroid Ni/NiO/C nanocomposite is attributed to the bicontinuous nature of gyroid structure that provide both short lithium diffusion distance and ideal electron transport paths.

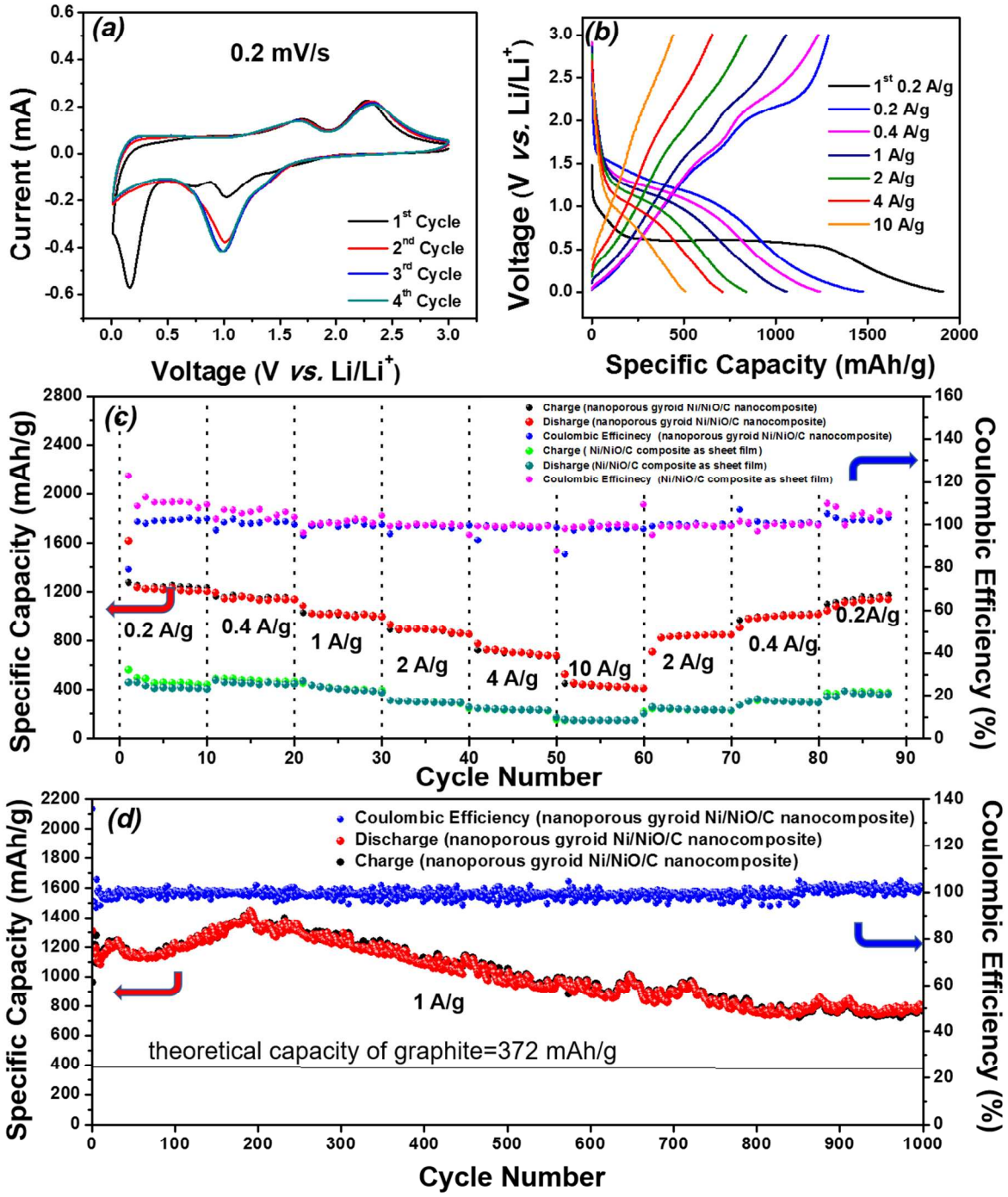

Figure. 4 Electrochemical performance of nanoporous gyroid Ni/NiO/C nanocomposite for LIBs (a) Cyclic voltammogram curves of the nanoporous gyroid Ni/NiO/C

nanocomposite anode collected at the scan rate of 0.2 mV/s within the voltage range of 0.005-3 V. (b) Charge/Discharge profiles at different current densities ranging from 0.2, 0.4, 1, 2, 4, 10 A/g as indicated. (c) Ratability test of gyroid Ni/NiO/C nanocomposite anode and sheet-film Ni/NiO/C composite anode. The electrode was charge/discharged for ten cycles under current densities from 0.2, 0.4, 1, 2, 4, 10, 2, 0.4 and 0.2 A/g as indicated. (d) Specific capacity of nanoporous gyroid Ni/NiO/C nanocomposite anode as a function of cycling number at the current density of 1 A/g (0.2 A/g was used for the initial four cycles to fully activate the electrode). The capacity retention of nanoporous gyroid Ni/NiO/C nanocomposite anode remains as high as 73% after 1000 cycles. The theoretical specific capacity of graphite was indicated in the figure as a black solid line.

The cycle performance of the nanoporous gyroid Ni/NiO/C nanocomposite anodes was further investigated. The data shown in Fig. 4(d) were recorded at 0.2 A/g for the initial four-cycles to fully activate the electrode, and then the data were collected at 1 A/g current density for the following cycles in the voltage range of 0.02–3.0 V (vs. Li/Li^+). The nanoporous gyroid Ni/NiO/C nanocomposite electrode exhibited excellent cycling stability with a capacity steadily increasing up to 1446 mAh/g after 191 cycles from the initial value of 1151 mAh/g. Furthermore, the rise in capacity was elucidated by the capacity plateaus changes of 60th, 90th, 120th, 150th and 180th cycles as shown in Fig. S12. The rise in capacity is not surprising for the nanostructured NiO-based electrode. This is usually explained by the gradual amorphization of crystalline NiO, which produces more Li ion accessible sites and improves kinetics for reoxidation of Ni to NiO.[22,72] The electrochemical impedance analysis of the nanoporous gyroid Ni/NiO/C nanocomposite electrode (see Supporting Information, Fig. S13) was conducted during

the long cycle test. As shown in Fig. S13, the EIS of initial anode and anode after 100, 400 and 800 cycles were presented. An equivalent circuit displayed in the inset of Fig. S13 was used to fit the spectra. The R_s represents the intrinsic resistance of the active materials, electrolyte and ionic resistance. The R_{sf} and CPE_{sf} relate to the resistance and the constant phase element of the SEI film, respectively; while the resistance and the constant phase element of the charge transfer are denoted as R_{cf} and CPE_{cf}, respectively. Additionally, W_o represents the Warburg element for diffusion of lithium ions. The fitting results were shown in Table S1. Note that the decrease of the R_{ct} with increasing charge/discharge cycle is in line with some reported literatures with NiO-based electrodes.[22, 24, 73] The decrease of the charge transfer resistance can be attributed to the feasibility of the charge transfer for the following cycles after the activation process is initially presented.[74] The specific capacity gradually decreased to 809 mAh/g after 1000 cycles, which was still 2.2 times higher than that of graphite anode (372mAh/g). The specific capacity retention after 1000 cycles was 73% and the average Coulombic efficiency reached 99.86%. The cyclability performance of the Ni/NiO/C composite materials with sheet-film morphology was collected for comparison. The long cycle tests showed that the sheet-film Ni/NiO/C anode was subject to a sudden capacity loss at the 187^{th} cycle. (Figure S11c) Such an abrupt capacity loss may be attributed to the loss of electrical contact with current collector, which is common observed during the pulverization of electrode materials. It is therefore evident that sheet-film Ni/NiO/C anode cannot mitigate the volume change issues of nickel oxide based conversion reaction type anode. The TEM image (Figure S14) of the nanoporous gyroid Ni/NiO/C nanocomposite after 1000 cycles showed that the original morphology of the electrode

materials was preserved, indicating a high stability of the active materials in the LIBs. As expected, by taking advantage of the unique network nanostructure, those nanoporous gyroid Ni/NiO/C nanocomposite anodes manifest high specific capacity and long-term cycling stability. We have compared with the cycling performance with previous reported NiO based anodes (see Supporting Information, Table S2), the gyroid Ni/NiO/C nanocomposite is among one of the most stable anodes.

Conclusions

In conclusion, a nanoporous gyroid Ni/NiO/C nanocomposite with well-ordered nanonetwork texture was successfully fabricated and developed as an electrode in the LIB applications. Following by the fabrication of gyroid-structured PS/Ni nanohybrids with templated electroless plating of Ni using nanoporous PS from self-assembled degradable BCPs template, a calcination process to degenerate PS template and oxidize Ni was conducted. The Ni/NiO composite with well reserved gyroid texture was used for carbon coating and produced nanoporous gyroid Ni/NiO/C nanocomposite that was further evaluated as the anode materials in LIB. Benefiting from the well-interconnected nanoporous structure with ultrafine transition metal oxide nanonetwork and uniform carbon coating, the gyroid Ni/NiO/C electrodes exhibited excellent specific capacity, ratability and cyclability. This work demonstrates the great potential of Ni/NiO/C nanocomposite with well-ordered nanonetwork textures in the design of high power LIBs. It is appealing to exploit the suggested approaches for the design and the development of high-rate capability electrodes in the future.

Conflict of Interest The authors declare no competing financial interest.

Acknowledgements The authors acknowledge Dr. B. Wang and Dr. M. Gao for the help with the SEM and TEM. The SEM observations using Quanta450 were carried out at the Liquid Crystal Institute Characterization Facility of Kent State University. The authors are grateful for financial support from The University of Akron. This work is supported by the National Science Foundation (NSF-CBET 1505943, 1706681 and NSF-DMR 1554851) and Ohio Federal Network Research (OFRN).

References

(1) A. S. Arico, P. Bruce, B. Scrosati, J.-M. Tarascon and W. V. Schalwkijk, *Nat. Mater.*, 2005, **4**, 366-377.

(2) M. R. Gao, Y. F. Xu, J. Jiang and Yu, S. H. *Chem. Soc. Rev.*, 2013, **42**, 2986-3017.

(3) K. Naoi, S. Ishimoto, J.-I. Miyamoto and W. Naoi, *Energy Environ. Sci.*, 2012, **5**, 9363-9373.

(4) Y.-G. Guo, J.-S. Hu and L.-J. Wan, *Adv. Mater.*, 2008, **20**, 2878-2887.

(5) C. Liu, F. Li, L. P. Ma and H. M. Cheng, *Adv. Energy Mater.*, 2010, **22**, E28.

(6) M. D. Stoller, S. Park, Y. Zhu, J. An and R. S. Ruoff, *Nano Lett.*, 2008, **10**, 3498-3502.

(7) B. Dunn, H. Kamath and J.-M. Tarasco, *Science*, 2011, **334**, 928-935.

(8) K. Kang, Y. S. Meng, J. Breger, C. P. Grey and G. Ceder, *Science*, 2006, **311**, 977-980.

(9) J. B. Goodenough and Y. Kim, *Chem. Mater.*, 2010, **22**, 587-603.

(10) S. Liu, Z. Wang, C. Yu, H. B. Wu, G. Wang, Q. Dong, J. Qiu, A. Eychmuller, X. W. Lou, *Adv. Mater.*, 2013, **25**, 3462-3467.

(11) L. Qie, W. M. Chen, Z. H. Wang, Q. G. Shao, X. Li, L. X. Yuan, X. L. Hu, W. X. Zhang and Y. H. Huang, *Adv. Mater.*, 2012, **24**, 2047-2050.

(12) Y. Yu, C. Yan, L. Gu, X. Lang, K. Tang, L. Zhang, Y. Hou, Z. Wang, M. W. Chen, O. G. Schmidt and J. Maier. *Adv. Energy Mater.*, 2013, **3**, 281-285.

(13) L. Zhang, H. B. Wu, B. Liu and X. W. Lou, *Energy Environ. Sci.*, 2014, **7**, 1013-1017.

(14) K. Cao, L. Jiao, H. Liu, Y. Liu, Y. Wang, Z. Guo and H. Yuan, *Adv. Energy Mater.*, 2015, **5**, 1401421.

(15) M. V. Reddy, G. V. Subba Rao and B. V. Chowdari, *Chem. Rev.*, 2013, **113**, 5364-5475.

(16) Y. Sun, X. Hu, W. Luo, F. Xia and Y. Huang, *Adv. Funct. Mater.*, 2013, **23**, 2436-2444.

(17) C. He, S. Wu, N. Zhao, C. Shi, E. Liu and J. Li, *ACS Nano*, 2013, **7**, 4459-4469.

(18) B. Jiang, Y. He, B. Li, S. Zhao, S. Wang, Y.-B. He, and Z. Lin, *Angew. Chem. Int. Ed.*, 2017, **56**, 1869 –1872.

(19) B. Jiang, C. Han, B. Li, Y. He, and Z. Lin, *ACS Nano*, 2016, **10**, 2728−2735.

(20) J. Liang, H. Hu, H. Park, C. Xiao, S. Ding, U. Paik and X. W. Lou, *Energy Environ. Sci.*, 2015, **8**, 1707-1711.

(21) F. Zou, Y. M. Chen, K. Liu, Z. Yu, W. Liang, S. M. Bhaway, M. Gao and Y. Zhu, *ACS Nano*, 2016, **10**, 377-386.

(22) X. Sun, W. Si, X. Liu, J. Deng, L. Xi, L. Liu, C. Yan and O. G. Schmidt, *Nano Energy*, 2014, **9**, 168-175.

(23) W. Guo, W. Sun and Y. Wang, *ACS Nano*, 2015, **9**, 11462-11471.

(24) X. Sun, C. Yan, Y. Chen, W. Si, J. Deng, S. Oswald, L. Liu and O. G. Schmidt, *Adv. Energy Mater.*, 2014, **4**, 1300912.

(25) S. Zhao, Z. Wang, Y. He, B. Jiang, Y. Harn, X. Liu, F Yu, F. Feng, Q. Shen, and Z. Lin, *ACS Energy Lett.*, 2017, 2, 111−116.

(26) Z. Gong and Y. Yang, *Energy Environ. Sci.*, 2011, **4**, 3223-3242.

(27) P. Roy and S. K. Srivastava, *J. Mater. Chem. A*, 2015, **3**, 2454-2484.

(28) P. G. Bruce, B. Scrosati and J. M. Tarascon, *Angew. Chem. Int. Ed.*, 2008, **47**, 2930-2946.

(29) L. Ji, Z. Lin, M. Alcoutlabi and X. Zhang, *Energy Environ. Sci.*, 2011, **4**, 2682-2699.

(30) Y. Kim, J.-H. Lee, S. Cho, Y. Kwon, I. In, J. Lee, N.-H. You, E. Reichmanis, H. Ko, K.-T. Lee, H.-K. Kwon, D.-H. Ko, H. Yang and B. Park. *ACS Nano*, 2014, **8**, 6701-6712.

(31) Z.-S. Wu, G. Zhou, L.-C. Yin, W. Ren, F. Li and H.-M. Cheng, *Nano Energy*, 2012, **1**, 107-131.

(32) Z. Wang, D. Luan, S. Madhavi, Y. Hu and X. W. Lou, *Energy Environ. Sci.*, 2012, **5**, 5252-5256.

(33) F. Zou, X. Hu, L. Qie, Y. Jiang, X. Xiong, Y. Qiao and Y. Huang, *Nanoscale*, 2014, **6**, 924-930.

(34) J. M. Jeong, B. G. Choi, S. C. Lee, K. G. Lee, S. J. Chang, Y. K. Han, Y. B. Lee, H. U. Lee, S. Kwon, G. Lee, C. Lee and Y. Huh. *Adv. Mater.*, 2013, **25**, 6250-6255.

(35) Z. Fan, J. Liang, W. Yu, S. Ding, S. Cheng, G. Yang, Y. Wang, Y. Xi, K. Xi and R. V. Kumar, *Nano Energy*, 2015, **16**, 152-162.

(36) H. Zhang, T. Shi, D. J. Wetzel, R. G. Nuzzo and P. V. Braun, *Adv. Mater.*, 2016, **28**, 742-747.

(37) X. Pang, Y. He, J. Jung, and Z. Lin, *Science*, 2016, **353**, 1268-1272.

(38) X. Pang, L. Zhao, W. Han, X. Xin and Z. Lin, *Nat. Nanotech.*, 2013 **8**, 426-431.

(39) F. S. Bates and G. H. Fredrickson, *Annu. Rev. Phys. Chem.*, 1990, **41**, 525-557.

(40) F. S. Bates and G. H. Block Fredrickson, *Phys. Today*, *1999*, **52**, 32-40.

(41) A. S. Zalusky, R. O. Valles, C. J. Taylor and M. A. Hillmyer, *J. Am. Chem. Soc.*, 2001, **123**, 1519-1520.

(42) W. H. Tseng, C. K. Chen, Y. W. Chiang, R. M. Ho, S. Akasaka and H. Hasegawa, *J. Am. Chem. Soc.*, **2009**, *131*, 1356-1357.

(43) Y. T. Tseng, W. H. Tseng, C. H. Lin and R. M. Ho, *Adv. Mater.*, 2007, **19**, 3584-3588.

(44) M. Park, C. Harrison, P. M. Chaikin, R. A. Register and D. H. Adamson, *Science*, *1997*, **276**, 1401-1404.

(45) T. T. Albrecht, R. Steiner, J. DeRouchey, C. M. Stafford, E. Huang, M. Bal, M. Tuominen, C. J. Hawker and T. P. Russell, *Adv. Mater.*, 2000, **12**, 787-791.

(46) J. Y. Cheng, C. A. Ross, V. Z. H. Chan, E. L. Thomas, R. G. H. Lammertink and G. J. Vancso, *Adv. Mater.*, 2001, **13**, 1174-1178.

(47) T. C. Lin, K. C. Yang, P Georgopanos, A. Avgeropoulos and R. M. Ho, *Polymer*, 2017, **126**, 360-367.

(48) H. Y. Hsueh, C. T. Yao and R. M. Ho, *Chem. Soc. Rev.*, 2015, **44**, 1974-2018.

(49) S. Grimm, R. Giesa, K. Sklarek, A. Langner, U. Gosele, H.-W. Schmidt and M. Steinhart, *Nano Lett.*, 2008, **8**, 1954-1959.

(50) F. Li, X. Yao, Z. Wang, W. Xing, W. Jin, J. Huang and Y. Wang, *Nano Lett.*, 2012, **12**, 5033-5038.

(51) E. J. W. Crossland, M. Kamperman, M. Nedelcu, C. Ducati, U. Wiesner, D. M. Smilgies, G. E. S. Toombes, M. A. Hillmyer, S. Ludwigs, U. Steiner and H. J. Snaith, *Nano Lett.*, 2009, **9**, 2807-2812.

(52) S. Guldin, I. Rushkin, M. Stefik, K. Hur, U. Wiesner, J. J. Baumber and U. Steiner, *Adv. Mater.*, 2011, **23**, 3664-3668.

(53) M. R. J. Scherer, L. Li, P. M. S. Cunha, O. A. Scherman and U. Steiner, *Adv. Mater.*, 2012, **24**, 1217-1221.

(54) H. Y. Hsueh, Y. C. Huang, R. M. Ho, C. H. Lai, T. Makida and H. Hasegawa, *Adv. Mater.*, 2011, **23**, 3041-3046.

(55) H. Y. Hsueh, H. Y. Chen, Y. C. Hung, Y. C. Ling, S. J. Gwo and R. M. Ho, *Adv. Mater.*, 2013, **25**, 1780-1786.

(56) C. F. Cheng, H. Y. Hsueh, C. H. Lai, C. J. Pan, B. J. Hwang, C. C. Hu and R. M. Ho, *NPG Asia Mater.*, 2015, **7**, e170.

(57) K. W. Liu, Y. M. Chen, G. M. Policastro, M. L. Becker and Y. Zhu, *ACS Nano*, 2015, **9**, 6041-6049.

(58) H. Y. Hsueh, H. Y. Chen, M. S. She, C. K. Chen, R. M. Ho, S. J. Gwo, H. Hasegawa and E. L. Thomas, *Nano. Lett.*, 2010, **10**, 4994-5000.

(59) H. Y. Hsueh and R. M. Ho, *Langmuir*, 2012, **28**, 8518-8529.

(60) Y. Wan and D. Zhao, *Chem. Rev.*, 2007, **107**, 2821-2860.

(61) J. Bella, R. Yeb, K. Ahmedc, C. Liu, M. Ozkanc and C. S. Ozkana, *Nano Energy*, 2015, **18**, 47-56.

(62) H. Y. Hsueh, Y. C. Ling, H. F. Wang, L.Y. C. Chien, Y. C. Hung, E. L. Thomas and R. M. Ho, *Adv. Mater.*, 2014, **26**, 3225-3229.

(63) F. Zou, X. Hu, Y. Sun, W. Luo, F. Xia, L. Qie, Y. Jiang and Y. Huang, *Chem. Eur. J.*, 2013, **19**, 6027-6033.

(64) A. N. Mansour, *Surf. Sci. Spectra*, 1994, **3**, 231–248.

(65) A. N. Mansour, *Surf. Sci. Spectra*, 1994, **3**, 239–246.

(66) H. Wang, X. Fan, X. Zhang, Y. Huang, Q. Wu, Q. Pana Q. Li, *RSC Adv*., 2017, **7**, 23328–23333.

(67) D. T. Dam, X. Wang and J.-M. Lee, *ACS Appl. Mater. Interfaces*, 2014, **6**, 8246-8256.

(68) M. A. Peck and M. A. Langell, *Chem. Mater.*, 2012, **24**, 4483-4490.

(69) W. Liu, C. Lu, X. Wang, K. Liang and B. K. Tay, *J. Mater. Chem. A*, 2015, **3**, 624-633.

(70) G. Zhou, D.-W. Wang, L.-C. Yin, N. Li, F. Li and H.-M. Cheng, *ACS Nano*, 2012, **6**, 3214-3223.

(71) X. Zheng, H. Wang, C. Wang, Z. Deng, L. Chen, Y. Lia, T. Hasan and B.-L. Su, *Nano Energy*, 2016, 22, 269.

(72) C. Peng, B. Chen, Y. Qin, S. Yang, C. Li, Y. Zuo, S. Liu and J. Yang, *ACS Nano*, 2012, **6**, 1074-1081.

(73) G. Huang, X. Guo, X. Cao, Q. Tian and H. Sun, *Nano Energy*, 2016, **28**, 338-345.

(74) B. Yan, M. Li, X. Li, Z. Bai, L. Dong and D. Li, *Electrochim. Acta*, 2015, **164**, 55-61.

Table of Content

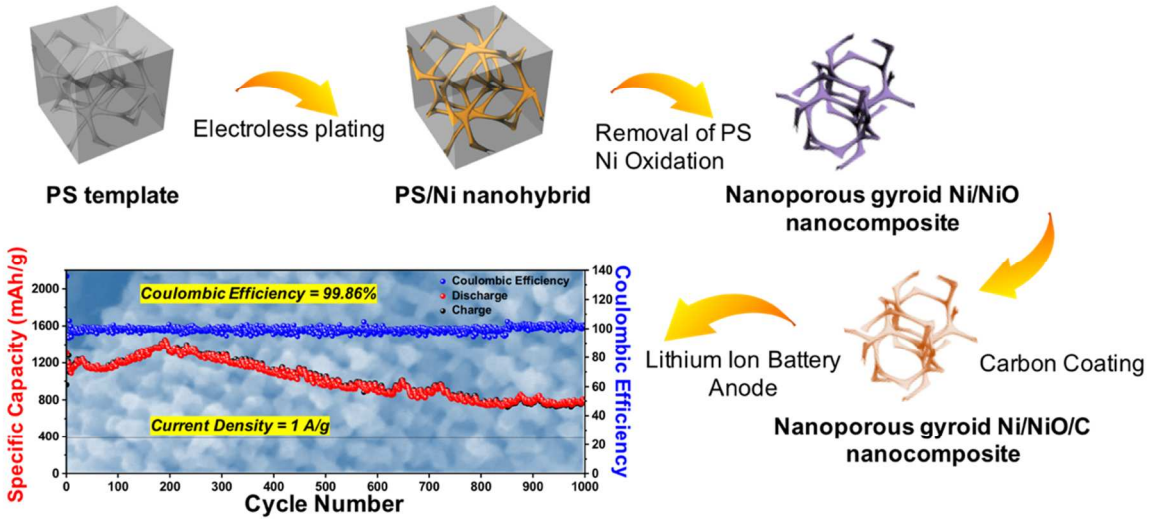

Nanoporous gyroid Ni/NiO/C nanocomposite electrode exhibited good cycle stability over 1000 cycles at 1 A/g with specific capacity of 800 mAh/g.